Available online at www.sciencedirect.com
SCIENCE DIRECT®
International Journal of Heat and Fluid Flow 25 (2004) 404–419
International Journal of HEAT AND FLUID FLOW
www.elsevier.com/locate/ijhff

Surface heat-flux fluctuations in a turbulent channel flow up to $Re_\tau = 1020$ with $Pr = 0.025$ and 0.71

Hiroyuki Abe [a], Hiroshi Kawamura [b,*], Yuichi Matsuo [a]

[a] Information Technology Center, Japan Aerospace Exploration Agency, Jindaiji-higashi, Chofu, Tokyo 182-8522, Japan
[b] Department of Mechanical Engineering, Tokyo University of Science, Noda-shi, Chiba 278-8510, Japan

Abstract

In the present study, direct numerical simulation of turbulent heat transfer in a channel flow has been carried out in order to investigate the characteristics of surface heat-flux fluctuations. The Reynolds numbers based on the friction velocity and the channel half width are 180, 395, 640 and 1020, and the molecular Prandtl numbers are 0.025 and 0.71. A local peak for $Pr = 0.71$ and large peaks for $Pr = 0.025$ appear in the spanwise-wavenumber power spectra at low wavenumbers, and these peaks become more significant with increasing Reynolds number. This suggests that the effect of large-scale structures extends even to the surface heat-flux fluctuations, and increases with increasing Reynolds number. In addition, it was found that the surface heat-flux fluctuations for $Pr = 0.71$ are mostly similar to the streamwise wall shear-stress fluctuations, while a noticeable dissimilarity can be seen in the large positive and negative fluctuations.

Keywords: Surface heat-flux fluctuations; Reynolds- and Prandtl-number dependence; Large-scale structure; Direct numerical simulation

1. Introduction

The behavior of wall variables in turbulent channel and boundary layer flows is of considerable interest in applications involving drag, noise and heat transfer. Recently, direct numerical simulation (DNS) has become an essential tool to examine turbulence phenomena, and several studies have used DNS to investigate the behavior of the wall variables. In the flow field, Choi and Moin (1990) examined the characteristics of the wall pressure fluctuations p_w for $Re_\tau = u_\tau\delta/\nu = 180$, where u_τ is the friction velocity, δ the channel half width, and ν the kinematic viscosity. Jeon et al. (1999) investigated the characteristics of two components of the wall shear-stress fluctuations, $\tau_1 = \mu(\partial u'/\partial y|_w)$ and $\tau_3 = \mu(\partial w'/\partial y|_w)$ for $Re_\tau = 180$, where u' and w' denote the streamwise and spanwise velocity fluctuations, respectively, μ the dynamic viscosity and y the distance from the wall. In these studies, the functional dependence of the mean-square values on Reynolds number and the scaling law of the power spectra have been fairly well examined as compared with results from the existing experimental data.

In the thermal field, Kim and Moin (1989) examined the behavior of the surface heat-flux fluctuations $q_w = a\rho c_p(\partial\theta'/\partial y|_w)$ for $Re_\tau = 180$ at $Pr = 0.71$ assuming constant heat generation throughout the fluid, where θ' denotes the temperature fluctuations, a the thermal diffusivity, ρ the density, and c_p the specific heat at constant pressure. They showed the root-mean-square value and the instantaneous field, and reported that the regions of high surface heat-flux coincide with the regions of high-speed fluid. On the other hand, the surface heat-flux is considered to be a modulation of the wall temperature, and there are several DNS studies on the wall temperature fluctuations (i.e. the near-wall limiting value of the temperature fluctuations) in a turbulent channel flow. Antonia and Kim (1991) investigated the near-wall limiting behavior for $Re_\tau = 180$ at $Pr = 0.1$, 0.71 and 2.0 using DNS database of Kim and Moin (1989). They indicated that the limiting value of the temperature fluctuations does not depend on the Prandtl number at $Pr \geqslant 0.1$. Kawamura et al. (1998) examined the Prandtl-number effect on turbulence statistics for $Re_\tau = 180$ at various Prandtl numbers ranging from

* Corresponding author. Tel.: +81-471-24-1501x3909; fax: +81-471-23-9814.
E-mail address: kawa@rs.noda.tus.ac.jp (H. Kawamura).

0142-727X/$ - see front matter © 2004 Elsevier Inc. All rights reserved.
doi:10.1016/j.ijheatfluidflow.2004.02.010

$Pr = 0.025$ to 5.0 with a constant time-averaged heat-flux condition. They showed that the limiting value of the temperature fluctuations depends strongly on the Prandtl number when Pr is less than 0.1. Kawamura et al. (1999) also investigated the Reynolds- and Prandtl-number effects on turbulence statistics for $Re_\tau = 180$ and 395 at $Pr = 0.025$, 0.2 and 0.71, and suggested that the Reynolds-number effect on the limiting value of the temperature fluctuations for $Pr = 0.025$ is significant, while those for $Pr = 0.2$ and 0.71 are rather small. Na and Hanratty (2000) examined the Prandtl-number effect on the near-wall limiting behavior for $Re_\tau = 180$ at higher Prandtl numbers, $Pr = 1.0$, 3.0 and 10.0 with a constant temperature difference condition. They showed the streamwise-wavenumber spectra of the temperature fluctuations normalized by their own mean-square values in close vicinity to the wall, and indicated that the contribution of high wavenumbers to the mean-square value decreases with increasing Prandtl number. Kowalewski et al. (2003) investigated the convection velocities of thermal structures in an open channel for $Re_\tau = 180$ at $Pr = 0.71$ and 5.4 with iso-thermal and iso-flux boundary conditions. They indicated that in the near-wall region the convection velocity of the temperature fluctuations at $Pr = 5.4$ is only about half of that for the streamwise velocity fluctuations. However, over $Re_\tau > 395$, the Reynolds- and Prandtl-number effects on the surface heat-flux (or the wall temperature) fluctuations from DNS have not been reported to date.

Recently, with the rapid increase in computer power, DNSs of turbulent channel flow have been carried out at relatively high Reynolds numbers (see, for example, Antonia and Kim, 1994; Moser et al., 1999; Abe et al., 2001; Iwamoto et al., 2002; Tanahashi et al., 2003; Satake et al., 2003). In addition, large-scale DNS has been performed on a turbulent channel flow for $Re_\tau = 550$ (del Álamo and Jiménez, 2001, 2003). As for turbulent heat transfer in a channel flow, the present authors' group has also performed large-scale DNS with a constant time-averaged heat-flux condition for $Re_\tau = 640$ with two Prandtl numbers of $Pr = 0.025$ and 0.71 (Abe and Kawamura, 2002). More recently, we have established DNS database of turbulent heat transfer in a channel flow for a higher Reynolds number of $Re_\tau = 1020$ with $Pr = 0.025$ and 0.71. To the authors' knowledge, DNS for $Re_\tau = 1020$ with $Pr = 0.025$ and 0.71 is the first DNS computation with turbulent heat transfer in a channel flow at a Reynolds number of $O(10^3)$.

In the present study, we have performed DNS of turbulent heat transfer in a channel flow, using our DNS database for four Reynolds numbers ($Re_\tau = 180$, 395, 640 and 1020) with two Prandtl numbers ($Pr = 0.025$ and 0.71) in order to examine the characteristics of the surface heat-flux fluctuations, where $Pr = 0.025$ and 0.71 are chosen to assume mercury and air, respectively, as the working fluids. The wide range of Reynolds numbers and the quite different Prandtl numbers give us a sound basis to investigate the Reynolds- and Prandtl-number effects. The objectives of the present study are to report the behavior of the surface heat-flux fluctuations as described by their root-mean-square values, power spectra, two-point correlations, space–time correlations, probability density functions and instantaneous fields, and to discuss the Reynolds- and Prandtl-number effects. Moreover, since u' shows almost the same behavior as θ' for $Pr = 0.71$ in the near-wall region with the present thermal boundary condition, high similarity is expected between τ_1 and q_w for $Pr = 0.71$, and this point is also discussed.

2. Numerical procedure

The flow is assumed to be a fully developed turbulent channel flow with a passive temperature field. It is driven by the streamwise mean pressure gradient. The temperature field is imposed by uniform heating at both walls with a constant time-averaged heat-flux. Note that in the present thermal boundary condition the average heat flux is constant but the instantaneous one is time dependent. All the variables computed from the Navier–Stokes and energy equations are normalized by the friction velocity u_τ, the friction temperature $T_\tau (= Q_w/\rho c_p u_\tau)$ and the channel half width δ, where Q_w is the given averaged surface heat flux.

In the present computation, a fractional step method proposed by Dukowics and Dvinsky (1992) is adopted, and a semi-implicit time advancement is used. For the viscous terms with wall-normal derivatives, the Crank–Nicolson method is used. For the other terms, the second-order Adams–Bashforth method is applied for $Re_\tau = 180$, 395 and 640, and the low storage third-order Runge–Kutta method (Spalart et al., 1991) for $Re_\tau = 1020$. For the spatial discretization, the finite difference method is used. The numerical scheme proposed by Morinishi et al. (1998) with the fourth-order accuracy is adopted in the streamwise and spanwise directions, whereas the second-order one is applied in the wall-normal direction. Detailed numerical procedures can be found in Kawamura et al. (2000) and Abe et al. (2001).

Several experimental studies in wall turbulence for high Reynolds numbers suggest that the contribution of the outer layer to the inner layer increases with increasing Reynolds number (for example, Naguib and Wark, 1992; Hites, 1997; Österlund, 1999). Moreover, recent DNS work by del Álamo and Jiménez (2001, 2003) at a relatively high Reynolds number of $Re_\tau = 550$ indicates that the effect of large-scale structures in the outer layer penetrates into the buffer region. Therefore, the size of the present computational domain was made as large as possible: $12.8\delta \times 2\delta \times 6.4\delta$ in the streamwise

Table 1
Computational box size, grid points, spatial resolution, calculation time step and sampling time period

Re_τ	180	395	640	1020
Pr	0.025, 0.71	0.025, 0.71	0.025, 0.71	0.025, 0.71
$L_x \times L_y \times L_z$	$12.8\delta \times 2\delta \times 6.4\delta$	$12.8\delta \times 2\delta \times 6.4\delta$	$12.8\delta \times 2\delta \times 6.4\delta$	$12.8\delta \times 2\delta \times 6.4\delta$
$L_x^+ \times L_y^+ \times L_z^+$	$2304\times360\times1152$	$5056\times790\times2528$	$8192\times1280\times4096$	$13\,056\times2040\times6528$
$N_x \times N_y \times N_z$	$256\times128\times256$	$512\times192\times512$	$1024\times256\times1024$	$2048\times448\times1536$
Δx^+, Δy^+, Δz^+	9.00, 0.20–5.90, 4.50	9.88, 0.15–6.52, 4.94	8.00, 0.15–8.02, 4.00	6.38, 0.15–7.32, 4.25
Δt^+	0.027	0.012	0.012	0.102
Tu_m/L_x	49	50	14	10

(x), wall-normal (y) and spanwise (z) directions, respectively, for all computational cases. The computational domain size $(L_x \times L_y \times L_z)$, number of grid points $(N_x \times N_y \times N_z)$, spatial resolution $(\Delta x, \Delta y, \Delta z)$, calculation time step (Δt) and sampling time period (Tu_m/L_x) are given in Table 1, where T and u_m are the sampling time and the bulk mean velocity, respectively.

3. Results and discussion

3.1. DNS results at $Re_\tau = 1020$

Before we discuss the behavior of the surface heat-flux fluctuations, the validation of DNS results at $Re_\tau = 1020$ is presented using conventional turbulence statistics. Fig. 1(a) shows the mean velocity distribution for $Re_\tau = 180$, 395, 640 and 1020. The experimental result of Wei and Willmarth (1989) at $Re_\tau \approx 1017$ and the DNS result of Moser et al. (1999) at $Re_\tau = 590$ are also included for comparison. In Fig. 1(a), agreement between the two results (the present study for $Re_\tau = 1020$ and Wei and Willmarth, 1989) is good. In addition, it can be seen that the intermediate region expands almost logarithmically with increasing Reynolds number, which also agrees with the result of Satake et al. (2003) for $Re_\tau = 1100$. The mean temperature distribution is given in Fig. 1(b) for $Re_\tau = 180$, 395, 640 and 1020 with $Pr = 0.025$ and 0.71, compared with the empirical formulas of Kader (1981) at $Re_\tau = 1020$ with the two Prandtl numbers. In Fig. 1(b), the present results at $Re_\tau = 1020$ agree well with the empirical formulas of Kader (1981) for both $Pr = 0.025$ and 0.71. For $Pr = 0.71$ the conductive sublayer is evident up to $y^+ \approx 5$ for each Reynolds number, and the intermediate region expands almost logarithmically with increasing Reynolds number, while for $Pr = 0.025$ only the conductive sublayer appears in the whole region independently of Reynolds number.

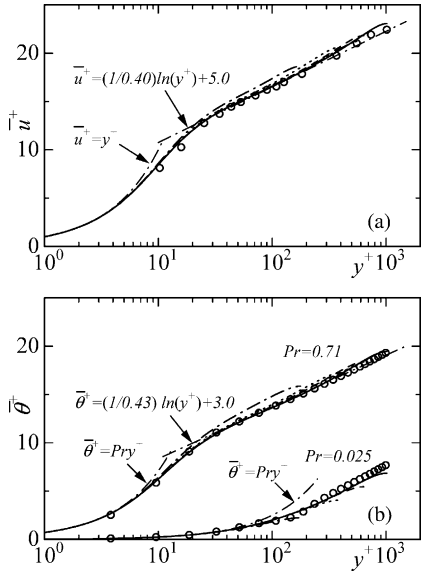

Fig. 1. Mean velocity and temperature distributions: —, $Re_\tau = 1020$; - - -, $Re_\tau = 640$; ⋯, $Re_\tau = 395$; –·–, $Re_\tau = 180$. (a) $\overline{u}^+$: –··–, Moser et al. (1999) for $Re_\tau = 590$; ○, Wei and Willmarth (1989) for $Re_\tau \approx 1017$; (b) $\overline{\theta}^+$: ○, Kader (1981) for $Re_\tau = 1020$.

The rms (root-mean-square) values of the streamwise velocity $(u'^+_{\rm rms})$ and the temperature fluctuations $(\theta'^+_{\rm rms})$ shown in Fig. 2(a) and (b), respectively, for the given Reynolds and Prandtl numbers. For the streamwise velocity fluctuations, agreement between the two results (the present study for $Re_\tau = 1020$ and Wei and Willmarth, 1989) is satisfactory except for the peak location where the measurement is extremely difficult. In addition, the peak value increases slightly with increasing Reynolds number. For the temperature fluctuations,

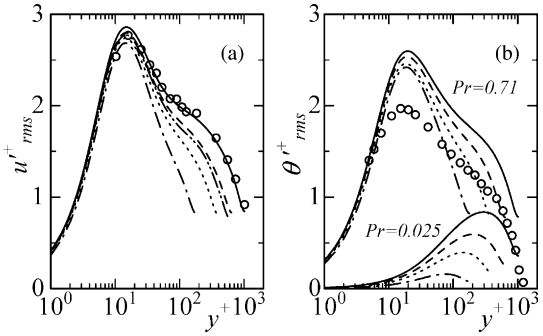

Fig. 2. Rms of streamwise velocity and temperature fluctuations: —, $Re_\tau = 1020$; - - -, $Re_\tau = 640$; ⋯, $Re_\tau = 395$; –·– $Re_\tau = 180$. (a) $u'^+_{\rm rms}$: –··–, Moser et al. (1999) for $Re_\tau = 590$; ○, Wei and Willmarth (1989) for $Re_\tau \approx 1017$; (b) $\theta'^+_{\rm rms}$: ○, Subramanian and Antonia (1981) for $Re_\tau \approx 1055$.

$\theta'^{+}_{\mathrm{rms}}$ for $Pr = 0.71$ shows almost the same Reynolds-number dependence as seen in u'^{+}_{rms}, while that for $Pr = 0.025$ increases considerably with increasing Reynolds number.

It should be noted that the total shear-stress and the total heat-flux reach statistically steady states for the given Reynolds and Prandtl numbers although they are not shown here. Detailed analysis on the turbulence statistics will be reported elsewhere.

3.2. Root-mean-square values

The root-mean-square (rms) values of the surface heat-flux fluctuations q_{w} normalized by the given averaged surface heat-flux Q_{w} for $Re_\tau = 180$, 395, 640 and 1020 with $Pr = 0.025$ and 0.71 are shown in Fig. 3. The streamwise wall shear-stress fluctuations τ_1 are also plotted for comparison. Note that in the DNS works referred in Fig. 3, Jeon et al. (1999) and Kim and Moin (1989) reported the rms values of τ_1 and q_{w}, respectively. Also, Antonia and Kim (1994) and Günther et al. (1998) gave the limiting values of the spanwise vorticity and the streamwise velocity fluctuations, respectively, i.e. $\tau_{1\mathrm{rms}}$. As in the rest of the DNS works, the rms values of τ_1 and q_{w} have been estimated from the limiting values of the spanwise vorticity and the temperature fluctuations, respectively, which can be obtained from their DNS database. In Fig. 3, the rms values of q_{w} increase with increasing Reynolds number for both of the Prandtl numbers. The increasing rate for $Pr = 0.025$ is larger than the one for $Pr = 0.71$ because of the increasing convective effect. Moreover, it is interesting to note that the rms value of q_{w} for $Pr = 0.025$ increases almost logarithmically with increasing Reynolds number. When the Reynolds number becomes $Re_\tau \gg 1000$, the rms value of q_{w} for $Pr = 0.025$ seems to exceed that of q_{w} for

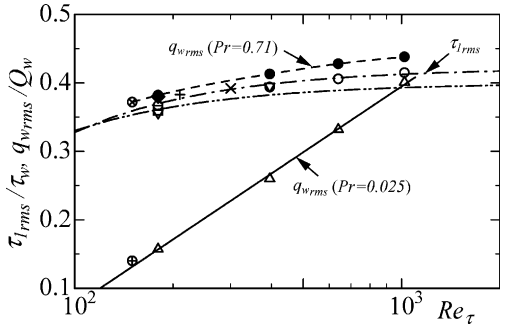

Fig. 3. Variations of the rms values of the streamwise wall shear-stress and surface heat-flux fluctuations as a function of the Reynolds number. ○, τ_1; ●, q_{w}, for $Pr = 0.71$; Δ, q_{w} for $Pr = 0.025$; ◆, Kim and Moin (1989); +, Gilbert and Kleiser (1991); ⊗, Kasagi et al. (1992); ⊕, Kasagi and Ohtsubo (1993); ▽, Antonia and Kim (1994); ×, Günther et al. (1998); □, Jeon et al. (1999); –·–, fitting for $\tau_{1\mathrm{rms}}/\tau_{\mathrm{w}}$ by Fischer et al. (2001) from DNS; –··–, fitting for $\tau_{1\mathrm{rms}}/\tau_{\mathrm{w}}$ by Fischer et al. (2001) from experiments; ---, fitting for $q_{\mathrm{w_{rms}}}/Q_{\mathrm{w}}$ for $Pr = 0.71$; —, fitting for $q_{\mathrm{w_{rms}}}/Q_{\mathrm{w}}$ for $Pr = 0.025$.

$Pr = 0.71$. This is because the effect of large scales is significant for $Pr = 0.025$, and increases considerably with increasing Reynolds number as discussed later.

As for τ_1, the present results agree well with those of other DNSs and with experiment. The value increases slightly with increasing Reynolds number and it seems to be nearly saturated at about $0.4\tau_{\mathrm{w}}$ at high Reynolds numbers. This trend corresponds to a recent experimental result by Metzger and Klewicki (2001), who examined the wall value of the spanwise vorticity fluctuation in a turbulent boundary layer at sufficiently high Reynolds numbers, although they showed a logarithmic increase in the peak value of u'_{rms}. A comparison between τ_1 and q_{w} with $Pr = 0.71$ reveals that the rms values of q_{w} are approximately 5% larger than those of τ_1 at each Reynolds number.

3.3. Power spectra

The power spectra of q_{w} are defined by

$$\int_0^\infty \phi(k_x)\,\mathrm{d}k_x = \int_0^\infty \phi(k_x)\,\mathrm{d}k_z = q^2_{\mathrm{w_{rms}}}, \tag{1}$$

where $\phi(k_x)$ and $\phi(k_z)$ are the power spectra, and k_x and k_z are the wavenumbers in the x and z directions, respectively. The streamwise- and spanwise-wavenumber power spectra of q_{w} normalized by the inner variables are given in Fig. 4. In the streamwise spectra, the spectra for $Pr = 0.71$ show good collapse at low and intermediate wavenumbers and power increases slightly with increasing Reynolds number at high wavenumbers, although for $Re_\tau = 180$ the spectra exhibit a noticeable Reynolds-number dependence. In contrast, the spectra for $Pr = 0.025$ do not show good collapse at the whole range of wavenumbers. With increasing Reynolds number, power increases significantly at low wavenumbers and also increases noticeably at intermediate and high wavenumbers.

Na and Hanratty (2000) suggested that in the close vicinity to the wall, the temperature fluctuations at high

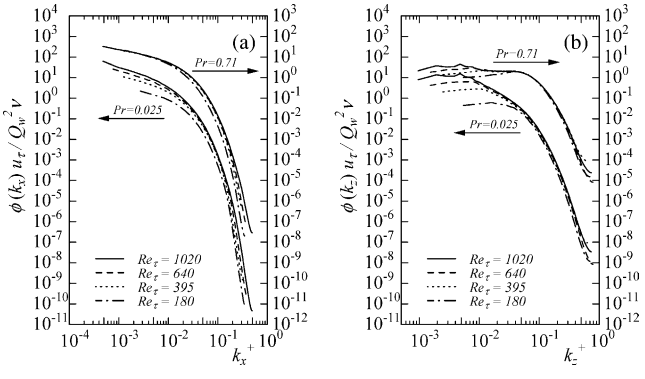

Fig. 4. One-dimensional wavenumber power spectra of q_{w} for $Pr = 0.025$ and 0.71 normalized by the inner variables: (a) streamwise wavenumber; (b) spanwise wavenumber.

Prandtl numbers are greatly damped by the molecular diffusion, which agrees with the finding of Campbell and Hanratty (1983). The same type of figure as that of Na and Hanratty (2000) is shown in Fig. 5, which gives the streamwise-wavenumber spectra of q_w normalized by their own mean-square values for $Re_\tau = 180$ and 1020 at $Pr = 0.025$ and 0.71 with the inner scaling. In Fig. 5, we see that the contribution of high wavenumbers (i.e. small scales) to the mean-square value decreases with decreasing Prandtl number for the given Reynolds numbers. Notably, this trend is more evident for $Re_\tau = 1020$. This result is in contrast to the finding of Na and Hanratty (2000), and the difference must be due to the different range of the Prandtl numbers. That is, the present work is concerned with the Prandtl numbers, $Pr < 1$, while Na and Hanratty (2000) considered the Prandtl numbers, $Pr \geqslant 1$. In the case of $Pr < 1$, small scales are gradually damped by the enhanced conductive effect with decreasing Prandtl number because the contribution of thermal diffusion increases. This trend can be seen in the instantaneous temperature field given later in Fig. 22(a) and (b). Accordingly, in the present Prandtl-number range, the contribution of high wavenumbers to the mean-square value decreases with decreasing Pr.

In the spanwise spectra, the spectra for $Pr = 0.71$ and 0.025 show almost the same Reynolds-number effect. That is, good collapse is found at intermediate and high wavenumbers, whereas power at low wavenumbers increases with increasing Reynolds number. However, the spectra exhibit a considerable Prandtl-number effect. In the case of $Pr = 0.71$, the spectra for $Re_\tau = 180$ show a peak at $k_z^+ \approx 0.038$ (corresponding to a wavelength of 165 wall units). The wavenumber of $k_z^+ \approx 0.038$ is slightly different from that of $k_x^+ \approx 0.063$ which corresponds to a spanwise spacing of near-wall streaky structures (i.e. 100 wall units). Considering the pre-multiplied spectra (not shown here) instead of the spanwise spectra, the maximum appears at $k_z^+ \approx 0.055$ (corresponding to a wavelength of 115 wall units), which is closer to the spanwise spacing of the streaks. This is because the peak location in the pre-multiplied spectrum corresponds to the wavelength of the energy-containing eddy (see, for example, Perry et al., 1986). With increasing Reynolds number, the power at low wavenumbers exceeds the power at $k_z^+ \approx 0.038$, indicating that in the spanwise direction a large-scale pattern becomes more significant with increasing Reynolds number rather than the near-wall streaky structure. In the case of $Pr = 0.025$, on the other hand, the spectra do not show a peak at an intermediate wavenumber for each Reynolds number, but show a maximum peak at a low wavenumber, suggesting that, in the case of $Pr = 0.025$, a streaky structure with a spanwise spacing of 100 wall units does not exist in the surface heat-flux fluctuations for the given Reynolds numbers, while a large-scale structure exists even in the surface heat-flux fluctuations.

Fig. 6 shows the streamwise- and spanwise-wavenumber power spectra of q_w normalized by the outer variables. For $Pr = 0.71$, the streamwise and spanwise spectra show a decrease in power at low wavenumbers with increasing Reynolds number, while showing an increase in power at high wavenumbers, indicating that the spectra for $Pr = 0.71$ are not scaled with the outer variables. In contrast, for $Pr = 0.025$, the streamwise and spanwise spectra show a systematic increase in power at low wavenumbers with increasing Reynolds number, which must result in a significant increase in the rms values. Therefore, the streamwise and spanwise spectra for $Pr = 0.025$, with outer scaling, are normalized by their own mean-square values and are shown in Fig. 7. In Fig. 7, the streamwise and spanwise spectra,

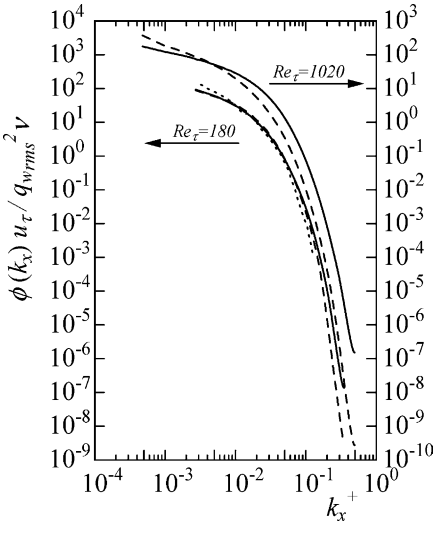

Fig. 5. One-dimensional streamwise wavenumber power spectra of q_w for $Re_\tau = 180$ and 1020 at $Pr = 0.025$ and 0.71 normalized by their own mean-square values with inner scaling: —, $Pr = 0.71$; - - -, $Pr = 0.025$; ···, θ' at $y^+ = 0.2$ of Na and Hanratty (2000) for $Re_\tau = 150$ at $Pr = 10.0$.

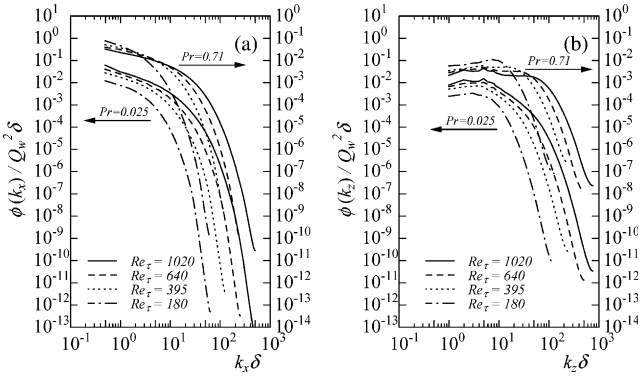

Fig. 6. One-dimensional wavenumber power spectra of q_w for $Pr = 0.025$ and 0.71 normalized by the outer variables: (a) streamwise wavenumber; (b) spanwise wavenumber.

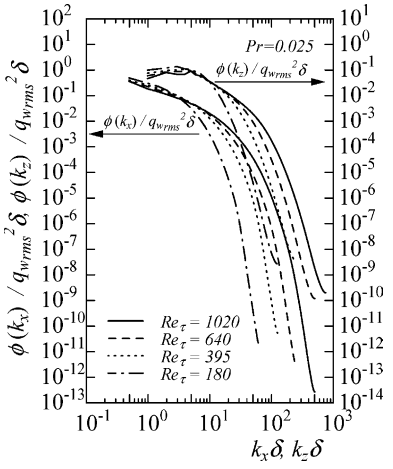

Fig. 7. One-dimensional wavenumber power spectra of q_w for $Pr = 0.025$ normalized by their own mean-square values with outer scaling.

non-dimensionalized by their own mean-square values, indeed show good collapse at low wavenumbers, suggesting that for $Pr = 0.025$, large scales are scaled well with the outer variables.

At low wavenumbers, a local peak is found for $Pr = 0.71$ with Reynolds numbers over $Re_\tau = 395$, while a maximum peak appears for $Pr = 0.025$ with the given Reynolds numbers (see Fig. 6(b)). The origin of the peaks observed in the spanwise spectra at low wavenumbers must be closely associated with large-scale motions (LSMs, hereafter) in the outer layer (see, for example, Robinson, 1991). Therefore, the spanwise spectra shown in Fig. 6 are presented again in Fig. 8 with linear scales. In the case of $Pr = 0.71$, a clear local peak appears at $k_z\delta \simeq 5$ (corresponding to a wavelength of 1.3δ) for the three Reynolds numbers, $Re_\tau = 395$, 640 and 1020, and it becomes more prominent with increasing Reynolds number. One may consider the local peak observed at the low wavenumber to be a numerical wiggle. We have taken this point into account and the computation for $Re_\tau = 395$ has been performed

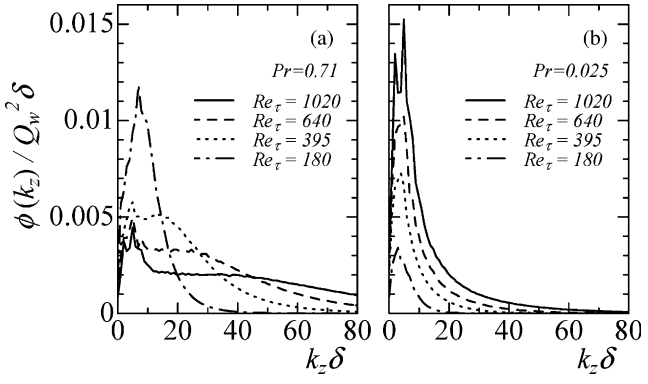

Fig. 8. One-dimensional spanwise-wavenumber power spectra of q_w normalized by Q_w and δ in linear scales: (a) $Pr = 0.71$; (b) $Pr = 0.025$.

with long sampling times such as 50 wash-out times. Moreover, a comparison of the results obtained from 25 and 50 wash-out times indicates that in both cases the local peak exists at the same low wavenumber. In the case of $Pr = 0.025$, on the other hand, two large peaks are observed at $k_z\delta \simeq 2$ and $k_z\delta = 4$–5 for $Re_\tau = 395$, 640 and 1020 and the peak at $k_z\delta = 4$–5 (corresponding to a wavelength of 1.3–1.6δ) shows a maximum for each Reynolds number. The values of these two peaks increase significantly with increasing Reynolds number. The wavelengths of the local peak for $Pr = 0.71$ and of the large peaks for $Pr = 0.025$ correspond to the wavelengths where the spanwise pre-multiplied power spectra in the outer layer show the most energetic power (not shown here), indicating that the effect of the LSMs in the outer layer extends even to the wall variables such as the surface heat-flux fluctuations. At the lowest Reynolds number, $Re_\tau = 180$, for $Pr = 0.71$ no peak is found at low wavenumbers but a maximum peak is found at $k_z\delta \simeq 7$ (corresponding to a wavelength of 165 wall units or 0.9δ), while, for $Pr = 0.025$, a large peak is found at $k_z\delta \simeq 3$ (corresponding to a wavelength of 378 wall units or 2.1δ). Since large and small scales are not clearly separated at $Re_\tau = 180$, this behavior must be attributed to the low Reynolds-number effect.

3.4. Two-point correlations

The streamwise and spanwise two-point correlations of q_w for $Re_\tau = 180$, 395, 640 and 1020 with $Pr = 0.71$ and 0.025 are given in Figs. 9 and 10. In Figs. 9 and 10, the separation distance for $Pr = 0.71$ and 0.025 is non-dimensionalized by the inner and outer variables, respectively. In the streamwise separation, when the Reynolds number is over $Re_\tau = 395$, the correlations for $Pr = 0.71$ extend to larger streamwise separations with increasing Reynolds number, whereas those for $Pr = 0.025$ do not show an appreciable Reynolds-number effect.

In the spanwise separation, for $Pr = 0.71$, the spanwise separation distance (in wall units) for maximum negative correlation is almost the same for all four Reynolds numbers, but the magnitude of the negative maximum decreases appreciably with increasing Reynolds number. Interestingly, as the Reynolds number reaches $Re_\tau = 1020$ a positive peak emerges at $z^+ \approx 110$. This trend is consistent with the behavior in the spanwise two-point correlations of the wall shear stress obtained from a recent experiment in a turbulent boundary layer at high Reynolds numbers by Österlund (1999). For $Pr = 0.025$, in contrast, the magnitude of maximum negative correlation is almost the same for all four Reynolds numbers, but the spanwise separation distance (in outer units) for the negative maximum moves slightly towards a smaller separation with increasing Reynolds number. At Reynolds numbers over $Re_\tau = 395$, the

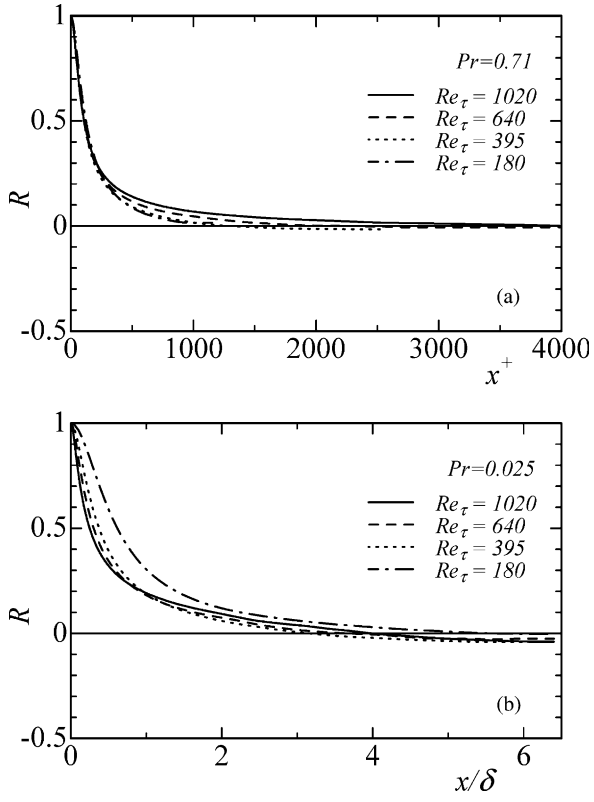

Fig. 9. Streamwise two-point correlation coefficients of q_w: (a) $Pr = 0.71$; (b) $Pr = 0.025$.

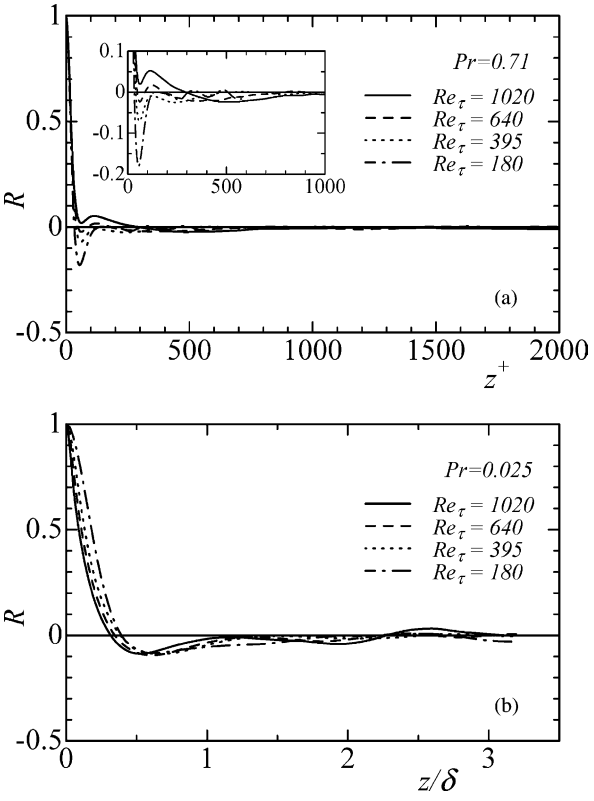

Fig. 10. Spanwise two-point correlation coefficients of q_w: (a) $Pr = 0.71$; (b) $Pr = 0.025$.

negative maximum correlation is clearly shown at $z/\delta \approx 0.65$, 0.60 and 0.52 for $Re_\tau = 395$, 640 and 1020, respectively. This behavior is caused by a variation of the contribution from the spanwise energetic scales as seen in Fig. 8(b).

At the lowest Reynolds number, $Re_\tau = 180$, a noticeable Reynolds-number dependence is found in the streamwise and spanwise two-point correlations for the two Prandtl numbers, which must be attributed to the low Reynolds-number effect.

3.5. Space–time correlations

Three-dimensional power spectra $\phi(k_x, k_z, \omega)$, where ω is the frequency, are computed with the same method of Choi and Moin (1990) in order to obtain space–time correlations. The data sets of 2048 and 4096 consecutive instantaneous surface heat-flux fluctuations have been used at time intervals of $\Delta t^+ = 0.99$ and 1.02 for $Re_\tau = 180$ and 1020, respectively. In the case of $Re_\tau = 180$, the total sampling number of 2048 is divided into 15 overlapping parts (50% overlap) with 256 frequency modes ($0 < \omega\delta/u_\tau < 566.7$), whereas, in the case of $Re_\tau = 1020$, the total sampling number of 4096 is divided into 7 overlapping parts (50% overlap) with 1024 frequency modes ($0 < \omega\delta/u_\tau < 3135.4$). With an integration of $\phi(k_x, k_z, \omega)$ in the spanwise direction, two-dimensional streamwise-wavenumber-frequency spectra $\phi(k_z, \omega)$ can be obtained. Then the space–time correlations of q_w can be obtained with an inverse Fourier transformation of $\phi(k_x, \omega)$, and are defined as

$$R(x,t) = \frac{\sum_{k_x} \sum_{\omega} \phi(k_x, \omega) e^{-ik_x x} e^{-i\omega t}}{q^2_{w_{rms}}}. \quad (2)$$

Fig. 11 shows the space–time correlations of q_w with $Pr = 0.025$ and 0.71 for two Reynolds numbers of $Re_\tau = 180$ and 1020, where the separations are non-dimensionalized by wall units. It is shown in Fig. 11 that the surface heat-flux fluctuations propagate downstream for the Reynolds and Prandtl numbers investigated. For $Pr = 0.71$, the correlations extend to larger streamwise ($x^+ > 1000$) and temporal ($t^+ > 100$) separations for the two Reynolds numbers. A noticeable Reynolds-number dependence is found only at the large separations, meaning that the effect of large-scale structures in the outer layer becomes more significant with increasing Reynolds number. In contrast, for $Pr = 0.025$, the space–time correlations show larger correlations at large separations compared with those for $Pr = 0.71$ with the two Reynolds numbers due to a strong conductive effect. Note that in Fig. 11(b) a noticeable correlation is found at the largest separations, which is attributed to the effect of the present computational domain. A comparison of the space–time correlations between $Pr = 0.71$ and 0.025 indicates that the inclination angle of the

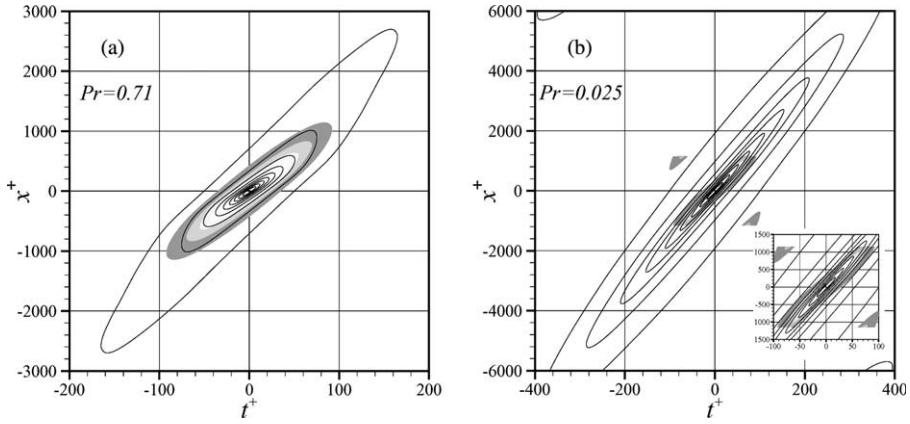

Fig. 11. Contours of space–time correlations of q_w: (a) $Pr = 0.71$; (b) $Pr = 0.025$. Line contours are for $Re_\tau = 1020$, whereas shaded contours are for $Re_\tau = 180$. Contour levels are from 0.1 to 0.9 with increments of 0.1.

correlations for $Pr = 0.025$ is much steeper than that of the correlations for $Pr = 0.71$, suggesting that q_w for $Pr = 0.025$ has a larger convection velocity than the one for $Pr = 0.71$.

Several methods are proposed to determine the convection velocity (see, for example, Wills, 1964; Choi and Moin, 1990; Kim and Hussain, 1993; Jeon et al., 1999). The ratio of streamwise and temporal separations where the space–time correlations show a maximum is usually used to obtain the convection velocity. The maximum correlation can be obtained in two ways, as a fixed time delay or a fixed streamwise separation. Convection velocities U_c^+ of q_w as functions of the temporal separation t^+ and the streamwise separation x^+ obtained from Fig. 11 are given in Fig. 12. It is apparent in Fig. 12 that the convection velocities of q_w for $Pr = 0.025$ are larger than those of q_w for $Pr = 0.71$ for the two Reynolds numbers. In the case of $Pr = 0.71$, the convection velocities as a function of t^+ show slightly lower values as compared to those as a function of x^+ due to the broad-band contours in the space–time correlations, but those convection velocities show an almost identical trend. At small separations, the convection velocities remain almost constant for the two Reynolds numbers, while, at large separations, the convection velocities for $Re_\tau = 180$ increase slightly but those for $Re_\tau = 1020$ increase significantly, meaning that the effect of large scales is more prominent for $Re_\tau = 1020$. In the case of $Pr = 0.025$, on the other hand, the convection velocities as functions of t^+ and x^+ show an almost identical behavior owing to the narrow-band contours in the space–time correlations. The convection velocities increase gradually with increasing separations for the two Reynolds numbers, and the Reynolds-number dependence is evident at all separations.

Overall convection velocity is a useful approximation in applying Taylor hypothesis. Wills (1964) proposed the overall convection velocity U_{c_o} expressed as

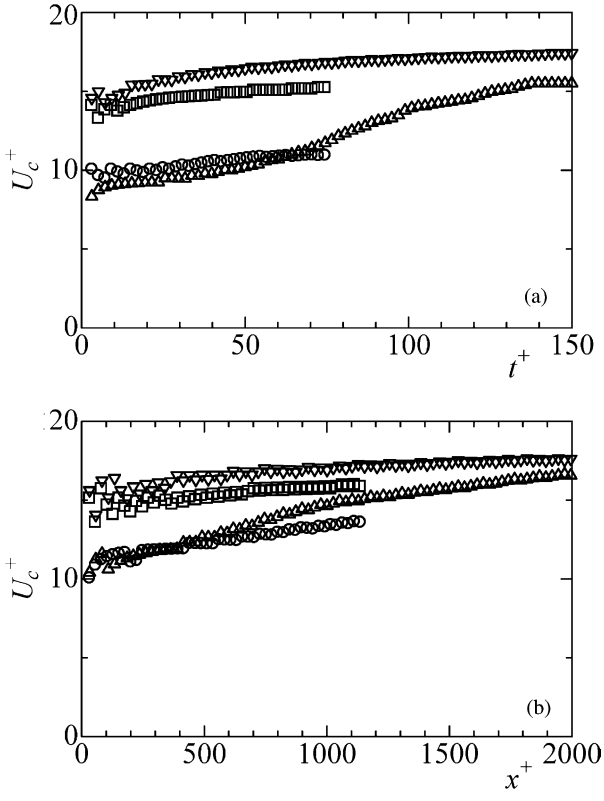

Fig. 12. Convection velocities U_c^+ of q_w as functions of t^+ and x^+: (a) temporal separation; (b) streamwise separation. ○, $Pr = 0.71$ for $Re_\tau = 180$; Δ, $Pr = 0.71$ for $Re_\tau = 1020$; □, $Pr = 0.025$ for $Re_\tau = 180$; ▽, $Pr = 0.025$ for $Re_\tau = 1020$.

$$U_{c_o} = \frac{\partial}{\partial U_c} \int R(U_c t, t)\, \mathrm{d}t \bigg|_{U_c = U_{c_o}} = 0. \tag{3}$$

Eq. (3) is satisfied when an integration time scale in the moving reference frame with the convection velocity shows a maximum. With the use of Eq. (3), the overall convection velocities of q_w with $Pr = 0.71$ are $10.5u_\tau$ and

$13.8u_\tau$ for $Re_\tau = 180$ and 1020, whereas those of q_w with $Pr = 0.025$ are $14.8u_\tau$ and $7.2u_\tau$ for $Re_\tau = 180$ and 1020, respectively.

The obtained overall convection velocities increase with increasing Reynolds number for the two Prandtl numbers. The significant increase in U_{c_o} for $Re_\tau = 1020$ can be predicted from Fig. 12, because the variation of the convection velocities becomes more prominent with increasing separations for $Re_\tau = 1020$. That is, the convection velocities obtained from Eq. (3) apply to all scales from small to large.

In order to remove scale dependence of the overall convection velocity, Kim and Hussain (1993) used the overall convection velocities U_{c_o} defined as

$$U_{c_o} = \frac{\Delta x_{\max}}{\Delta t}, \tag{4}$$

where $\Delta x_{\max}$ is the streamwise separation distance where the space–time correlations show a maximum correlation at a given time Δt. In the present study, $\Delta t^+ \approx 18$ was chosen for the given Reynolds and Prandtl numbers, as in Kim and Hussain (1993). With the use of Eq. (4), the overall convection velocities of q_w with $Pr = 0.71$ are $10.1u_\tau$ and $9.4u_\tau$ for $Re_\tau = 180$ and 1020, whereas those of q_w with $Pr = 0.025$ are $14.1u_\tau$ and $15.3u_\tau$ for $Re_\tau = 180$ and 1020, respectively. For $Re_\tau = 180$, the convection velocities obtained from Eq. (4) are almost the same as obtained from Eq. (3) for the two Prandtl numbers, a similarity that must be due to be the low Reynolds-number effect because small and large scales are not clearly separated at $Re_\tau = 180$. In contrast, for $Re_\tau = 1020$, the convection velocities obtained from Eq. (4) are significantly lower than those obtained from Eq. (3) for the Prandtl numbers investigated.

We will examine which overall convection velocity obtained from Eqs. (3) and (4) is valid for $Re_\tau = 1020$. Fig. 13 shows the streamwise-wavenumber spectra converted from the frequency spectra using Taylor hypothesis for $Re_\tau = 1020$ with $Pr = 0.71$ and 0.025. In Fig. 13, the streamwise-wavenumber spectra as shown in Figs. 4(a) and 6(a) are also included for comparison. In the case of $Pr = 0.71$, the spectrum obtained using the overall convection velocity from Eq. (4) shows good agreement with the wavenumber spectrum at the nearly whole range of wavenumbers, whereas that obtained using the overall convection velocity from Eq. (3) does not agree with the wavenumber spectrum at the whole range of wavenumbers. In the case of $Pr = 0.025$, the spectrum obtained using the overall convection velocity from Eq. (4) shows better agreement with the wavenumber spectra at high wavenumbers than that with the overall convection velocity obtained from Eq. (3). Hence, at the Reynolds number of $Re_\tau = 1020$, it can be concluded that the overall convection velocities obtained from Eq. (4) are more appropriate than those obtained from Eq. (3).

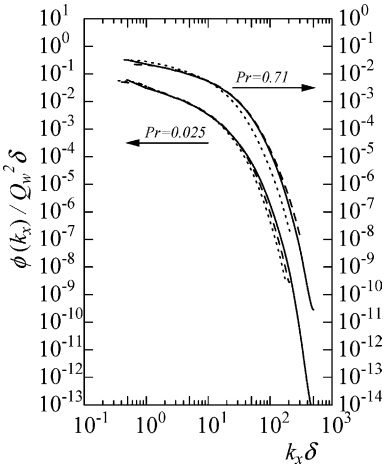

Fig. 13. One-dimensional streamwise-wavenumber power spectra of q_w converted from frequency spectra using Taylor hypothesis for $Re_\tau = 1020$ with $Pr = 0.71$ and 0.025: —, streamwise-wavenumber spectra; - - -, spectra converted from frequency spectra using the convection velocity obtained from Eq. (4); ⋯, spectra converted from frequency spectra using the convection velocity obtained from Eq. (3).

In summary, the overall convection velocities increase with decreasing Prandtl number for the two Reynolds numbers, which agrees with the trend obtained from DNS in a turbulent flume by Kowalewski et al. (2003), who investigated the overall convection velocity of θ' with working fluids of air and water at $Re_\tau = 171$. This is because large scales become more prominent with decreasing Prandtl number and convection of large scales is determined by the outer layer. As for the Reynolds-number dependence, on the other hand, the convection velocities obtained from Eq. (4) for $Pr = 0.71$ decrease slightly with increasing Reynolds number, whereas those for $Pr = 0.025$ increase slightly with increasing Reynolds number.

3.6. Probability density function

The behavior of the surface heat-flux fluctuations q_w was investigated with the use of the probability density functions (PDFs). Fig. 14 shows the PDFs of q_w for all four Reynolds numbers, $Re_\tau = 180$, 395, 640 and 1020 with $Pr = 0.025$ and 0.71, compared with those of τ_1. It is shown in Fig. 14 that sweep motion occurs less frequently, but contributes more significantly to the heat transport for both of the Prandtl numbers. The Reynolds-number effect is evident in the positive and negative tails of the PDFs for both of the Prandtl numbers. In addition, a comparison of Fig. 14(a) and (b) reveals that the PDFs of q_w for $Pr = 0.71$ are mostly similar to those of τ_1, while there exists some dissimilarity between τ_1 and q_w at positive and negative tails. That is, in the positive tail, the PDF of q_w for $Pr = 0.71$ shows a larger value than that of τ_1, indicating that q_w is more positively skewed in space than τ_1. This trend is in accor-

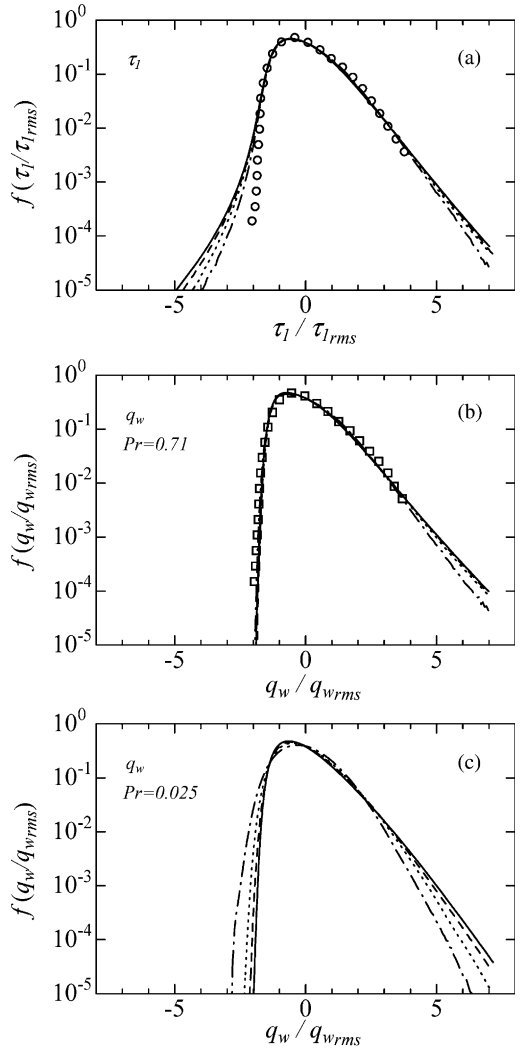

Fig. 14. Probability density functions of the streamwise wall shear-stress and surface heat-flux fluctuations: (a) τ_1; (b) q_w for $Pr = 0.71$; (c) q_w for $Pr = 0.025$. —, $Re_\tau = 1020$; - - -, $Re_\tau = 640$; ···, $Re_\tau = 395$; –·–, $Re_\tau = 180$. ○, u' at $y^+ \simeq 2.7$ of Antonia et al. (1988) for $Re_{\delta_2} = 2000$; □, θ' at $y^+ \simeq 2.7$ of Antonia et al. (1988) for $Re_{\delta_2} = 2000$.

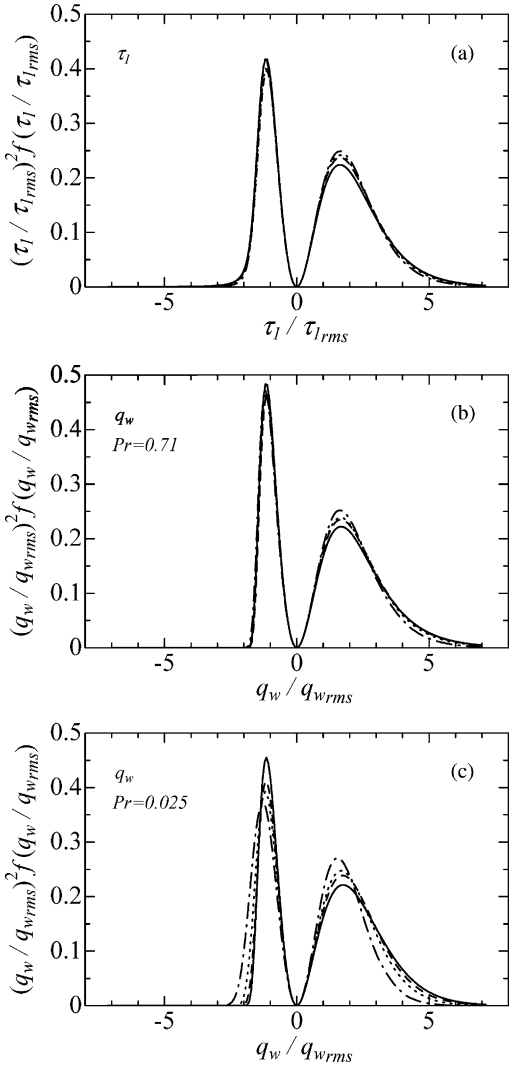

Fig. 15. Fractional contributions of the mean-square values: (a) τ_1; (b) q_w for $Pr = 0.71$; (c) q_w for $Pr = 0.025$. —, $Re_\tau = 1020$; - - -, $Re_\tau = 640$; ···, $Re_\tau = 395$; –·–, $Re_\tau = 180$.

dance with a measurement in a turbulent thermal boundary layer by Antonia et al. (1988) where they showed the PDFs of u' and θ' at $y^+ = 2.7$ for $Re_{\delta_2} = 2000$ ($Re_{\delta_2} = 2085$, for the present result at $Re_\tau = 1020$). Note that Re_{δ_2} is the Reynolds number based on the free-stream velocity and the momentum thickness. In the negative tail, in contrast, an interesting behavior is clearly observed, that is, the PDF of τ_1 extends to $\tau_1/\tau_{1\mathrm{rms}} = -5$, whereas that of q_w stays within $q_w/q_{w_{\mathrm{rms}}} = -2$. The reason will be discussed later in conjunction with the wall pressure fluctuations.

The fractional contributions of the mean-square values are shown in Fig. 15, where the integration of the area under the curve corresponds to 1. It can be seen in Fig. 15 that the contribution of positive values to $q_{w_{\mathrm{rms}}}$ is much larger than that of negative values for both of the Prandtl numbers. A significant Reynolds-number dependence is found for $Pr = 0.025$ due to the enhanced convective effect. In addition, a comparison of Fig. 15(a) and (b) again reveals the dissimilarity between τ_1 and q_w with $Pr = 0.71$ in the negative side. That is, the small magnitude of negative q_w ($q_w/q_{w_{\mathrm{rms}}} \approx -1$) contributes more significantly to the mean-square values than that of negative τ_1 ($\tau_1/\tau_{1\mathrm{rms}} \approx -1$).

Higher-order turbulence statistics, skewness and flatness factors of τ_1 and q_w, are shown in Fig. 16(a) and (b), respectively. Those of u' at $y^+ = 0.05$ of Moser et al. (1999) are also included for comparison. For $Pr = 0.71$, $S(q_w)$ and $F(q_w)$ increase slightly with increasing Reynolds number. A comparison of q_w and τ_1 reveals that $S(q_w)$ is more positively skewed than $S(\tau_1)$ for the given Reynolds numbers, which coincides with the behavior of PDFs (see Fig. 14(a) and (b)). Moreover, $F(q_w)$ shows larger values than $F(\tau_1)$, indicating that q_w is more

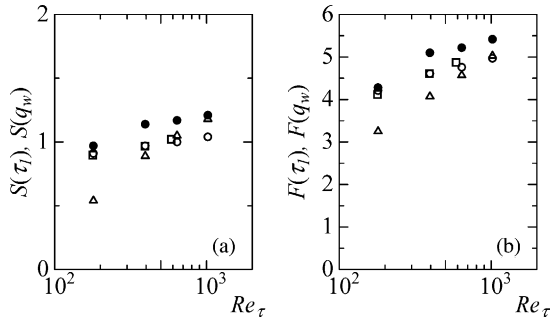

Fig. 16. Skewness and flatness factors of τ_1 and q_w: (a) skewness factor; (b) flatness factor. ○, τ_1; ●, q_w for $Pr = 0.71$; △, q_w for $Pr = 0.025$; □, u' at $y^+ = 0.05$ of Moser et al. (1999).

intermittent than τ_1. For $Pr = 0.025$, in contrast, $S(q_w)$ and $F(q_w)$ increase significantly with increasing Reynolds number. The increasing rates of $S(q_w)$ and $F(q_w)$ for $Pr = 0.025$ is much larger than those for $Pr = 0.71$, indicating that with increasing Reynolds number, the convective effect becomes more significant than the conductive one for $Pr = 0.025$. It is interesting to note that in the case of $Re_\tau = 1020$, the values of $S(q_w)$ and $F(q_w)$ for $Pr = 0.025$ is almost the same as those for $Pr = 0.71$, even if their turbulent heat fluxes themselves are different.

In order to examine the correlations between flow and thermal fields, the joint probability density function between τ_1 and q_w is given in Fig. 17. For $Pr = 0.71$, a strong positive correlation between τ_1 and q_w is found, but for $Pr = 0.025$, q_w is less well correlated with τ_1 due to a strong conductive effect. Fig. 17 also shows that the correlations at higher magnitude fluctuations decrease with increasing Reynolds number for both of the Prandtl numbers. Moreover, a closer inspection of the case $Pr = 0.025$ finds that the maximum in the third quadrant shifts away from the origin with increasing Reynolds number. This is caused by the enhanced convective effect even in a low Pr fluid.

As was shown in the probability density functions (Figs. 14 and 15), there exists some dissimilarity between τ_1 and q_w with $Pr = 0.71$ in the large positive and negative tails. The large negative tails showed an especially noticeable difference. This difference must be closely associated with the large wall pressure fluctuations because the importance of the pressure in causing the dissimilarity between the momentum and thermal fields has been indicated by several researchers (see, for example, Guezennec et al., 1990; Kong et al., 2001). Therefore, we will examine the statistical quantities related to the wall pressure fluctuations such as $\overline{\tau_1 p_w}$ and $\overline{q_w p_w}$ for the two Reynolds numbers, $Re_\tau = 180$ and 640, where p_w denotes the wall pressure fluctuations. The resultant values of $\overline{\tau_1 p_w}$ for $Re_\tau = 180$ and 640 are 0.05 and 0.10, whereas those of $\overline{q_w p_w}$ for $Re_\tau = 180$ and 640 are −0.05 and −0.11, respectively. Here, it is interesting to note that the values of $\overline{\tau_1 p_w}$ are positive, whereas those of $\overline{q_w p_w}$ are negative for both Reynolds numbers.

In order to examine the difference in $\overline{\tau_1 p_w}$ and $\overline{q_w p_w}$ with $Pr = 0.71$ in detail, we will use the quadrant analysis. The fractional contribution and probability distribution of $\overline{\tau_1 p_w}$ and $\overline{q_w p_w}$ from each quadrant for $Re_\tau = 180$ and 640 are summarized in Tables 2 and 3. Note that $(\overline{\tau_1 p_w})_j$ and $(\overline{q_w p_w})_j$ are the fractional contribution from the jth quadrant and $P(\overline{\tau_1 p_w})_j$ and $P(\overline{q_w p_w})_j$ are the probability of the jth quadrant. It is indeed found that the contributions to $\overline{\tau_1 p_w}$ are more significant in the first $(\tau_1 > 0, p_w > 0)$ and third $(\tau_1 < 0, p_w < 0)$ quadrants for both Reynolds numbers, which produces the positive value in $\overline{\tau_1 p_w}$. The contributions to $\overline{q_w p_w}$, on the other hand, are from the second $(q_w < 0, p_w > 0)$ and fourth $(q_w > 0, p_w < 0)$ quadrants, which produces

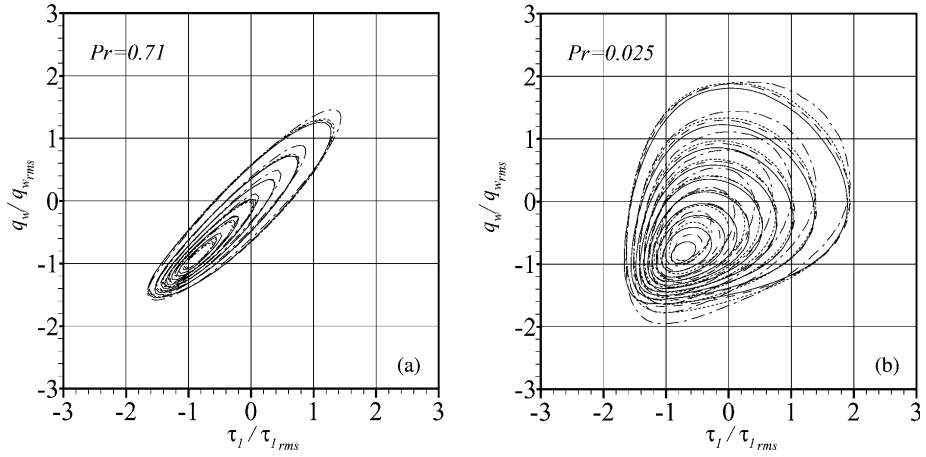

Fig. 17. Joint probability density functions of the streamwise wall shear-stress and surface heat-flux fluctuations: (a) $Pr = 0.71$; (b) $Pr = 0.025$. —, $Re_\tau = 1020$; - - -, $Re_\tau = 640$; ···, $Re_\tau = 395$; –·–, $Re_\tau = 180$. Contour levels for $Pr = 0.71$ are from 0.1 to 0.6 with increments of 0.1, while those for $Pr = 0.025$ are from 0.025 to 0.225 with increments of 0.025.

Table 2
Fractional contribution and probability distribution of $\overline{\tau_1 p_w}$ and $\overline{q_w p_w}$ at $Pr = 0.71$ from each quadrant for $Re_\tau = 180$

Event	$(\overline{\tau_1 p_w})_j$	$P(\overline{\tau_1 p_w})_j$	$(\overline{q_w p_w})_j$	$P(\overline{q_w p_w})_j$
$j = 1$	0.10	0.23	0.08	0.21
$j = 2$	−0.07	0.27	−0.10	0.29
$j = 3$	0.10	0.29	0.08	0.27
$j = 4$	−0.08	0.21	−0.11	0.23

Table 3
Fractional contribution and probability distribution of $\overline{\tau_1 p_w}$ and $\overline{q_w p_w}$ at $Pr = 0.71$ from each quadrant for $Re_\tau = 640$

Event	$(\overline{\tau_1 p_w})_j$	$P(\overline{\tau_1 p_w})_j$	$(\overline{q_w p_w})_j$	$P(\overline{q_w p_w})_j$
$j = 1$	0.17	0.23	0.13	0.20
$j = 2$	−0.10	0.27	−0.16	0.30
$j = 3$	0.16	0.30	0.12	0.27
$j = 4$	−0.13	0.20	−0.20	0.23

the negative value in $\overline{q_w p_w}$. These results indicate that the high dissimilarity between τ_1 and q_w with $Pr = 0.71$ is closely associated with the wall pressure fluctuations.

The contours of the instantaneous p_w, τ_1 and q_w with $Pr = 0.71$ for $Re_\tau = 640$ are shown in Fig. 18. It is clear from Fig. 18 that the positive and negative regions of q_w are mostly similar to those of τ_1. However, there is the noticeable dissimilarity between τ_1 and q_w in the large wall pressure fluctuations. The dissimilarity is especially clear in the large negative p_w. In Fig. 18, the typical events of the dissimilarity are marked by A and B. In these events, the large negative regions of τ_1 correspond to those of p_w, which produces the positive value of $\overline{\tau_1 p_w}$. In contrast, the large positive and small negative regions of q_w correspond to the large negative regions of p_w, which produces the negative value of $\overline{q_w p_w}$. Here, it should be noted that when a large negative τ_1 appears, there is a large negative p_w, but the reverse is not necessarily true. In addition, it is interesting to note that the magnitude of the negative q_w remains unchanged even with the large positive and negative p_w. This behavior results in the large difference in the negative tails of the PDFs between τ_1 and q_w.

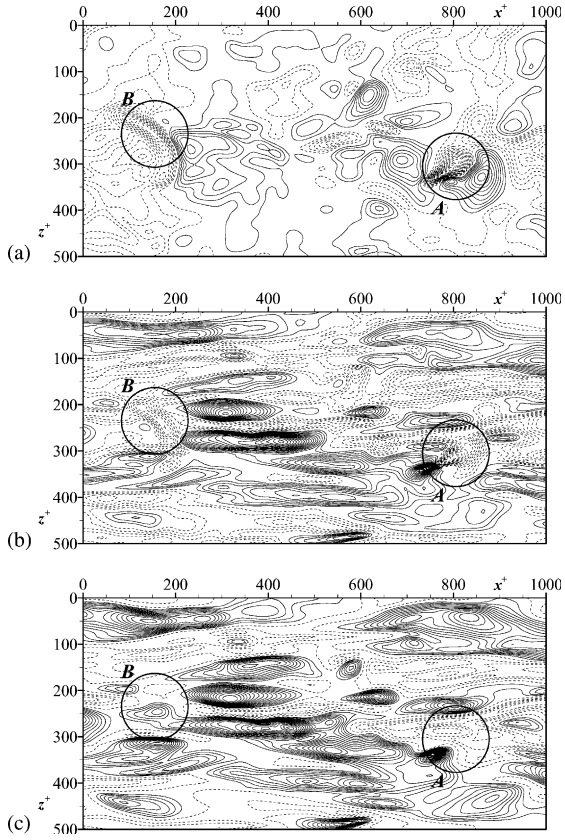

Fig. 18. Contours of the instantaneous p_w, τ_1 and q_w with $Pr = 0.71$ for $Re_\tau = 640$: (a) p_w (contours are from −9.0 to 19.0 with increments of 1.0); (b) τ_1 (contours are from −1.3 to 1.9 with increments of 0.1); (c) q_w at $Pr = 0.71$ (contours are from −0.7 to 2.5 with increments of 0.1). Positive values are solid lines, whereas negative values are dashed lines.

3.7. Instantaneous fields

We will show a variation of the instantaneous field as a function of the Reynolds number. Fig. 19 shows the contours of the instantaneous surface heat-flux fluctuations q_w for all four Reynolds numbers, $Re_\tau = 180$, 395, 640 and 1020 with $Pr = 0.71$ over the full computational domain. It can be seen in Fig. 19 that with increasing Reynolds number negative regions of q_w tend to show dense clustering structures. This behavior is more clearly illustrated in Fig. 20, where the contours of q_w with $Pr = 0.71$ are shown for $Re_\tau = 180$ and 1020 with a similarly visualized domain in wall units ($L_x^+ \times L_z^+ = 2000 \times 1000$). In Fig. 20, the negative regions of q_w for $Re_\tau = 180$ show clear streaky structures with a mean spanwise spacing of about 100 wall units, whereas those of q_w for $Re_\tau = 1020$ show dense clustering structures where several meandering negative regions merge. This results in the peculiar behavior of the spanwise two-point correlations that the magnitude of the negative maximum at $z^+ \approx 55$ decreases with increasing Reynolds number and the positive peak emerges at $z^+ \approx 110$ for $Re_\tau = 1020$ (Fig. 10(a)). Moreover, the dense clustering structures exhibit a large-scale pattern in the spanwise direction. The large-scale pattern is clearly observed in the cases of $Re_\tau = 640$ and 1020 (see Fig. 19(c) and (d)). The most typical large-scale pattern has a spanwise spacing of about 1.3–1.6δ, which agrees with the wavelength where the spanwise power spectra show the local peak (see Fig. 8(a)).

Fig. 21 shows the contours of the instantaneous surface heat-flux fluctuations q_w for the given Reynolds numbers with $Pr = 0.025$ over the full computational domain. In Fig. 21, the thermal structures show large-scale structures scaled with the outer variable δ for all four Reynolds numbers. At the lowest Reynolds

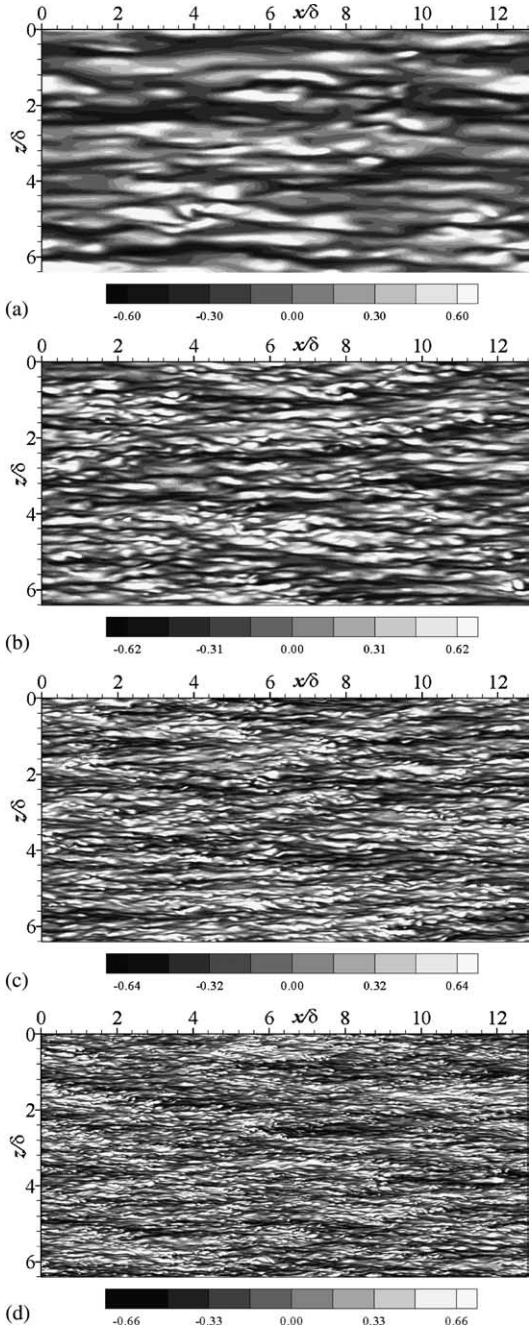

Fig. 19. Contours of the instantaneous q_w with $Pr = 0.71$: (a) $Re_\tau = 180$; (b) $Re_\tau = 395$; (c) $Re_\tau = 640$; (d) $Re_\tau = 1020$.

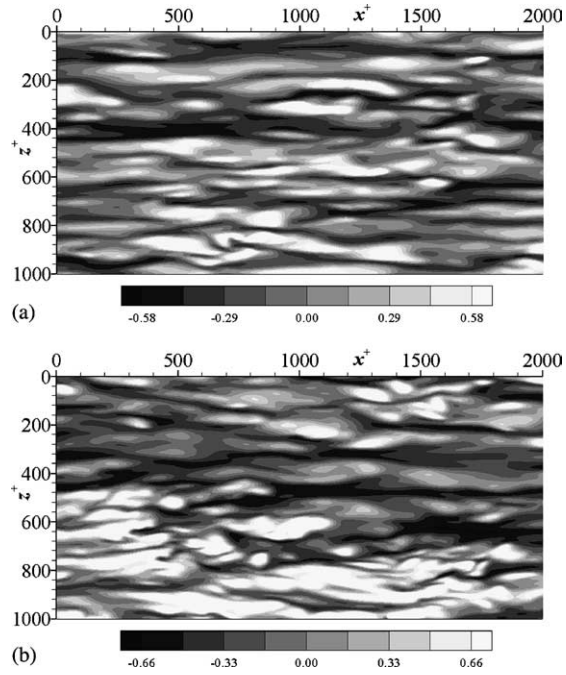

Fig. 20. Contours of the intantaneous q_w with $Pr = 0.71$ with a similarly visualized domain in wall units: (a) $Re_\tau = 180$; (b) $Re_\tau = 1020$.

number, $Re_\tau = 180$, large-scale structures with a spanwise spacing of about 2δ dominate. At Reynolds numbers over $Re_\tau = 395$, large-scale structures with a spanwise spacing of about 1.3–1.6δ are prominent. The spanwise spacing of these large-scale structures corresponds well to the wavelengths in the large peaks as shown in the spanwise power spectra (see Fig. 8(b)).

We will examine the effect of the outer layer from the instantaneous field for $Re_\tau = 1020$. Fig. 22(a) and (b) show the iso-surfaces of large-scale structures of θ' in the outer layer for $Re_\tau = 1020$ with $Pr = 0.71$ and 0.025, respectively. In Fig. 22, the values for $Pr = 0.71$ are normalized by their own rms values at each wall-normal location, whereas those for $Pr = 0.025$ are non-dimensionalized by wall units. This is because in the former case the strong intensities arise in the near-wall region, while in the latter case they occur farther away from the wall (see Fig. 2(b)). It is shown in Fig. 22 that there certainly exist large-scale structures in the outer layer for both of the Prandtl numbers. Notably, in the case of $Pr = 0.025$, the large-scale structures appear clearly in the outer layer, and they extend down to the wall. This is because in the case of $Pr = 0.025$, the temperature marks a wider range of the flow region due to the strong thermal diffusion. A comparison of Fig. 22(a) and (b) indicates that positive and negative large-scale structures for $Pr = 0.71$ show a strong similarity to those for $Pr = 0.025$, although the shape of the structures for $Pr = 0.71$ becomes more complicated than those of the structures for $Pr = 0.025$ due to the strong convective effect. Moreover, we see that the large-scale structures of θ' in the outer layer occur at almost the same locations as observed in the large-scale patterns of q_w for $Pr = 0.71$ and the large-scale structures of q_w for $Pr = 0.025$, indicating that the outer-layer effect certainly extends to the surface heat-flux fluctuations.

To examine the interaction between the inner and outer layers for $Re_\tau = 1020$ with $Pr = 0.71$ and 0.025 quantitatively, we introduce a function called an overlap ratio (OLR). In the OLR, variables ϕ and ψ are binarized to be either 0 or 1 based on a certain threshold, and

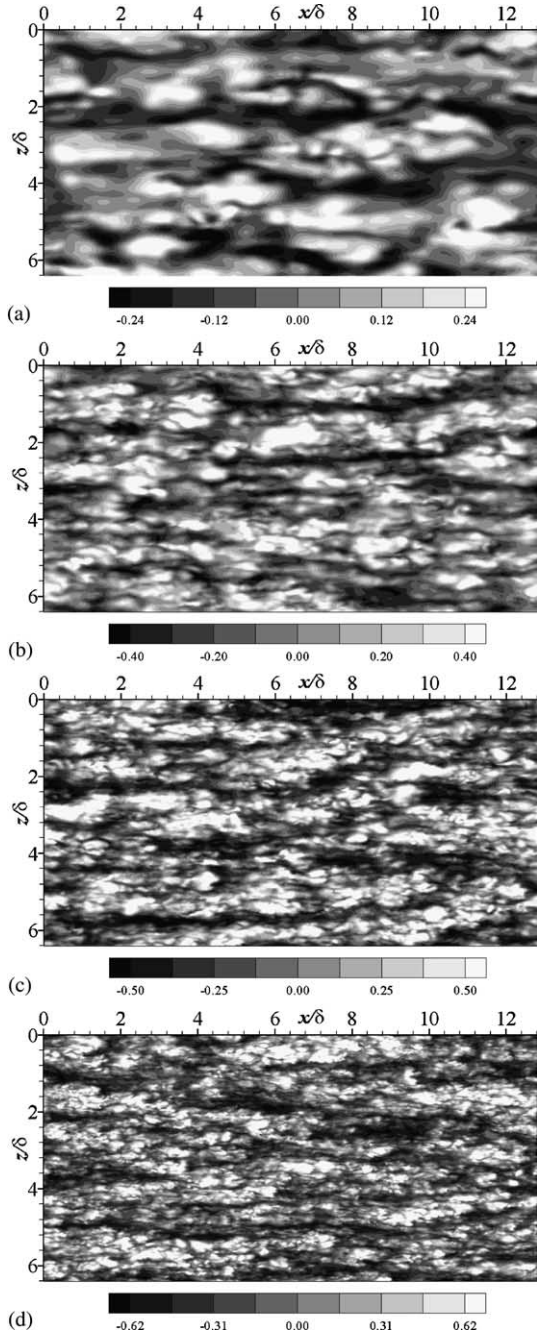

Fig. 21. Contours of the intantaneous q_w with $Pr = 0.025$: (a) $Re_\tau = 180$; (b) $Re_\tau = 395$; (c) $Re_\tau = 640$; (d) $Re_\tau = 1020$.

the binarized ones are represented by $\hat{\phi}$ and $\hat{\psi}$. Then, the OLR is defined as the ratio of the overlapping area between $\hat{\phi}$ and $\hat{\psi}$ to the area of either $\hat{\phi}$ or $\hat{\psi}$:

$$\mathrm{OLR}(\phi < \phi_0 \text{ or } \phi > \phi_0 \mid \psi < \psi_0 \text{ or } \psi > \psi_0) = \sum \hat{\phi}\hat{\psi} \Big/ \sum \hat{\psi}^2, \quad (5)$$

where ϕ_0 and ψ_0 are the threshold values. We obtain the OLR between the surface heat-flux fluctuations q_w and the projected area of high or low regions of θ' in the

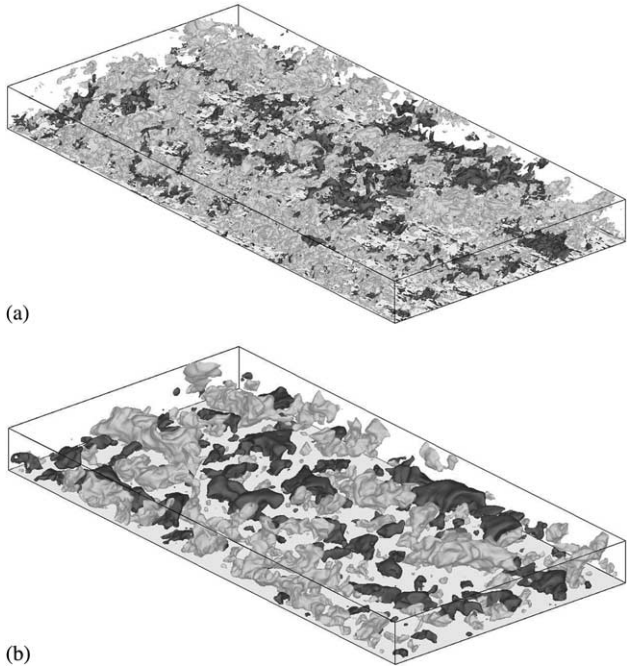

Fig. 22. Iso-surfaces of large-scale structures of θ' in the outer layer for $Re_\tau = 1020$; (a) $Pr = 0.71$; (b) $Pr = 0.025$. Dark-gray, $\theta/\theta'_{rms} < -1.75$ for $Pr = 0.71$ and $\theta'^{+} < -1.0$ for $Pr = 0.025$; light-gray, $\theta/\theta'_{rms} > 1.75$ for $Pr = 0.71$ and $\theta'^{+} > 1.0$ for $Pr = 0.025$. The box visulaized here is $12.8\delta \times \delta \times 6.4\delta$ in the steamwise, wall-normal and spanwise directions, corresponding to that of $13\,056 \times 1020 \times 6528(\nu/u_\tau)^3$. The direction of the flow is from top-left to bottom-right.

LSMs, where the filtered q_w (i.e. $\tilde{q}_w$) and the instantaneous q_w are used for $Pr = 0.71$ and 0.025, respectively, where a top-hat filter function with the streamwise and spanwise filter lengths of $\ell_x^+ = 293$ and $\ell_z^+ = 47$, respectively, is applied to the instantaneous q_w for $Pr = 0.71$. First, the surface heat-flux fluctuations for $Pr = 0.71$ and 0.025 are binarized with thresholds of $\tilde{q}_{w_0}/\tilde{q}_{w_{rms}} = \pm 1.5$ and $q_{w_0}/q_{w_{rms}} = \pm 1.5$, respectively. Next, the high and low regions for $Pr = 0.71$ and 0.025 are binarized with respect to $\theta'_0/\theta'_{rms} = \pm 1.75$ and $\theta'_0/T_\tau = \pm 1.0$, respectively, and the binarized values are projected onto the wall and then re-binarized as 0 or 1. The OLRs obtained between the high- and low-temperature regions in the LSMs and the positive and negative regions of q_w for $Re_\tau = 1020$ are summarized in Tables 4 and 5 with $Pr = 0.71$ and 0.025, respectively. Tables 4 and 5 show that the correspondence between the inner and outer layer structures is indeed high for each Prandtl number.

Table 4
Overlap ratio between the high- and low-temperature regions in the LSMs and the positive and negative regions of $\tilde{q}_w$ for $Re_\tau = 1020$ with $Pr = 0.71$

$\mathrm{OLR}(\theta' < -1.75\theta'_{rms} \mid \tilde{q}_w < -1.5\tilde{q}_{w_{rms}})$	0.83
$\mathrm{OLR}(\theta' < -1.75\theta'_{rms} \mid \tilde{q}_w > 1.5\tilde{q}_{w_{rms}})$	0.34
$\mathrm{OLR}(\theta' < 1.75\theta'_{rms} \mid \tilde{q}_w > 1.5\tilde{q}_{w_{rms}})$	0.73
$\mathrm{OLR}(\theta' < 1.75\theta'_{rms} \mid \tilde{q}_w < -1.5\tilde{q}_{w_{rms}})$	0.24

Table 5
Overlap ratio between the high- and low-temperature regions in the LSMs and the positive and negative regions of q_w for $Re_\tau = 1020$ with $Pr = 0.025$

OLR($\theta' < -1.0T_\tau \| q_w < -1.5q_{w_{rms}}$)	0.83
OLR($\theta' < -1.0T_\tau \| q_w < 1.5q_{w_{rms}}$)	0.06
OLR($\theta' > 1.0T_\tau \| q_w > 1.5q_{w_{rms}}$)	0.63
OLR($\theta' > 1.0T_\tau \| q_w < -1.5q_{w_{rms}}$)	0.08

4. Conclusions

In the present study, we performed DNS of turbulent heat transfer in a channel flow with the constant time-averaged heat-flux condition up to $Re_\tau = 1020$ with $Pr = 0.025$ and 0.71, and investigated the characteristics of the surface heat-flux fluctuations.

We found that the root-mean-square values increase with increasing Reynolds number for the two Prandtl numbers. The rate of increase for $Pr = 0.025$ is larger than that for $Pr = 0.71$ because of the increasing convective effect. Although the rms values for $Pr = 0.025$ showed smaller values than those for $Pr = 0.71$ in the present Reynolds-number range, the rms value of q_w for $Pr = 0.025$ seems to exceed that of q_w for $Pr = 0.71$ when the Reynolds number becomes $Re_\tau \gg 1000$.

It was shown in the power spectra and the two-point correlations that the Reynolds-number dependence is less significant when scaled with the inner and outer variables for $Pr = 0.71$ and 0.025, respectively. Especially, in the case of $Pr = 0.025$, it is evident that large scales are scaled well with the outer variables. Moreover, it was shown in the spanwise power spectra that, in the case of $Pr = 0.71$, there appears a clear local peak at $k_z\delta \simeq 5$ for $Re_\tau = 395$, 640 and 1020, whereas, in the case of $Pr = 0.025$, two large peaks exist at $k_z\delta \simeq 2$ and $k_z\delta = 4$–5 for $Re_\tau = 395$, 640 and 1020. These local and large peaks increase with increasing Reynolds number. This result suggests that the effect of large-scale structures extend even to the surface heat-flux fluctuations and becomes more prominent with increasing Reynolds number.

It was shown in the space–time correlations that the surface heat-flux fluctuations propagate downstream for the Reynolds and Prandtl numbers investigated. A comparison of the space–time correlations between $Pr = 0.71$ and 0.025 indicated that the inclination angle of the correlations for $Pr = 0.025$ is much steeper than that of the correlations for $Pr = 0.71$, suggesting that q_w for $Pr = 0.025$ has a larger convection velocity than the one for $Pr = 0.71$. The overall convection velocities of q_w with $Pr = 0.71$ are $10.1u_\tau$ and $9.4u_\tau$ for $Re_\tau = 180$ and 1020, whereas those of q_w with $Pr = 0.025$ are $14.1u_\tau$ and $15.3u_\tau$ for $Re_\tau = 180$ and 1020, respectively.

It was found in the probability density function that there is some dissimilarity between τ_1 and q_w with $Pr = 0.71$ in the large positive and negative tails. The large negative tails showed an especially noticeable difference. The examination of the dissimilarity between τ_1 and q_w showed that q_w are mostly similar to τ_1, while there exists a noticeable dissimilarity in the large positive and negative fluctuations. Closer inspection showed that a high dissimilarity between τ_1 and q_w exists in the large wall pressure fluctuations.

The instantaneous fields showed that, in the case of $Pr = 0.71$, large-scale patterns with dense clustering structures appear for high Reynolds numbers, whereas, in the case of $Pr = 0.025$, large-scale structures with the outer variable δ are dominant. In addition, inspection of the interaction between inner and outer layers revealed that the positive and negative dominant regions in q_w correspond to the high- and low-temperature regions in the LSMs for both of the Prandtl numbers. These results indicate that the large-scale structures in the surface heat-flux fluctuations are essentially phenomena associated with the LSMs for the thermal field existing in the outer layer.

Ensemble averaged statistics are/will be presented at http://murasun.me.noda.tus.ac.jp.

Acknowledgements

The present work is based on an earlier study of the wall shear stress fluctuations, in which the contribution by Prof. H. Choi of Seoul National University was significant. Computations were made with VPP5000 at Tokyo University of Science and Computer Center of Kyushu University, and also Numerical Simulator III at Computer Center of Japan Aerospace Exploration Agency.

References

Abe, H., Kawamura, H., 2002. A study of turbulence thermal structure in a channel flow through DNS up to $Re_\tau = 640$ with $Pr = 0.025$ and 0.71. In: Proc. of 9th European Turbulence Conference, pp. 399–402.

Abe, H., Kawamura, H., Matsuo, Y., 2001. Direct numerical simulation of a fully developed turbulent channel flow with respect to the Reynolds number dependence. ASME J. Fluids Eng. 123, 382–393.

Antonia, R.A., Kim, J., 1991. Turbulent Prandtl number in the near-wall region of a turbulent channel flow. Int. J. Heat Mass Transfer 34 (7), 1905–1908.

Antonia, R.A., Kim, J., 1994. Low-Reynolds-number effects on near-wall turbulence. J. Fluid Mech. 276, 61–80.

Antonia, R.A., Krishnamoorthy, L.V., Fulachier, L., 1988. Correlation between the longitudinal velocity fluctuation and temperature fluctuation in the near-wall region of a turbulent boundary layer. Int. J. Heat Mass Transfer 31 (4), 723–730.

Campbell, J.A., Hanratty, T.J., 1983. Mechanism of turbulent mass transfer at a solid boundary. AIChE J. 29 (2), 221–228.

Choi, H., Moin, P., 1990. On the space–time characteristics of wall pressure fluctuations. Phys. Fluids A 2, 1450–1460.

del Álamo, J.C., Jiménez, J., 2001. Direct numerical simulation of the very anisotropic scales in a turbulent channel. In: Center for turbulence Research Annual Research Briefs, pp. 329–341.

del Álamo, J.C., Jiménez, J., 2003. Spectra of the very large anisotropic scales in turbulent channels. Phys. Fluids 15 (6), L41–L44.

Dukowics, J.K., Dvinsky, A.S., 1992. Approximate factorization as a high order splitting for the implicit incompressible flow equations. J. Comp. Phys. 102, 336–347.

Fischer, M., Jovanović, J., Durst, F., 2001. Reynolds number effects in the near-wall region of turbulent channel flows. Phys. Fluids 13, 1755–1767.

Gilbert, N., Kleiser, L., 1991. Turbulence model testing with the aid of direct numerical simulation results. In: Proc. of the Eighth Symposium on Turbulent Shear Flows, TU of Munich, pp. 26.1.1–26.1.6.

Guezennec, Y., Stretch, D., Kim, J., 1990. The structure of turbulent channel flow with passive scalar transport. In: Center for turbulence Research Proceedings of the Summer Program, pp. 127–138.

Günther, D.V., Papavassiliou, D.D., Warholic, M.D., Hanratty, T.J., 1998. Turbulent flow in a channel at low Reynolds number. Exp. Fluids 25, 503–511.

Hites, M.H., 1997. Scaling of High-Reynolds Number Turbulent Boundary Layers in the National Diagnostic Facility. Ph.D. Thesis, Illinois Inst. of Technology.

Iwamoto, K., Suzuki, Y., Kasagi, N., 2002. Reynolds number effect on wall turbulence: toward effective feedback control. Int. J. Heat Fluid Flow 23, 678–689.

Jeon, S., Choi, H., Yoo, J.Y., Moin, P., 1999. Space–time characteristics of the wall shear-stress fluctuations in a low-Reynolds-number channel flow. Phys. Fluids 11, 3084–3094.

Kader, B.A., 1981. Temperature and concentration profiles in fully turbulent boundary layers. Int. J. Heat Mass Transfer 24 (9), 1541–1544.

Kasagi, N., Ohtsubo, Y., 1993. Direct numerical simulation of low Prandtl number thermal field in a turbulent channel flow. In: Durst, et al. (Eds.), Turbulent Shear Flows 8. Springer-Verlag, Berlin, pp. 97–119.

Kasagi, N., Tomita, Y., Kuroda, A., 1992. Direct numerical simulation of passive scalar field in a turbulent channel flow. ASME J. Heat Transfer 114, 598–606.

Kawamura, H., Ohsaka, K., Abe, H., Yamamoto, K., 1998. DNS of turbulent heat transfer in channel flow with low to medium-high Prandtl number fluid. Int. J. Heat Fluid Flow 19, 482–491.

Kawamura, H., Abe, H., Matsuo, Y., 1999. DNS of turbulent heat transfer in channel flow with respect to Reynolds and Prandtl number effects. Int. J. Heat Fluid Flow 20, 196–207.

Kawamura, H., Abe, H., Shingai, K., 2000. DNS of turbulence and heat transport in a channel flow with different Reynolds and Prandtl numbers and boundary conditions. In: Nagano et al. (Eds.), Proc. of 3rd Int. Symp. Turbulence, Heat and Mass Transfer, pp. 15–32.

Kim, J., Hussain, F., 1993. Propagation velocity of perturbations in turbulent channel flow. Phys. Fluids A 5, 695–706.

Kim, J., Moin, P., 1989. Transport of passive scalars in a turbulent channel flow. In: André, et al. (Eds.), Turbulent Shear Flows 6. Springer-Verlag, Berlin, pp. 85–96.

Kong, H., Choi, H., Lee, J.S., 2001. Dissimilarity between the velocity and temperature fields in a perturbed turbulent thermal boundary layer. Phys. Fluids 13 (5), 1466–1479.

Kowalewski, T.A., Mosyak, A., Hetsroni, G., 2003. Tracking of coherent thermal structures on a heated wall. 2. DNS simulation. Exp. Fluids 34, 390–396.

Metzger, M.M., Klewicki, J.C., 2001. A comparative study of near-wall turbulence in high and low Reynolds number boundary layers. Phys. Fluids 13 (3), 692–701.

Morinishi, Y., Lund, T.S., Vasilyev, O.V., Moin, P., 1998. Fully conservative higher order finite difference schemes for incompressible flow. J. Comp. Phys. 143, 90–124.

Moser, R.D., Kim, J., Mansour, N.N., 1999. Direct numerical simulation of turbulent channel flow up to $Re_\tau = 590$. Phys. Fluids 11, 943–945.

Na, Y., Hanratty, T.J., 2000. Limiting behavior of turbulent scalar transport close to a wall. Int. J. Heat Mass Transfer 43 (10), 1749–1758.

Naguib, A.M., Wark, C.E., 1992. An investigation of wall-layer dynamics using a combined temporal filtering and correlation technique. J. Fluid Mech. 243, 541–560.

Österlund, J.M., 1999. Experimental Studies of Zero Pressure-Gradient Turbulent Boundary Layer Flow. Ph.D. Thesis, Department of Mechanics, Royal Institute of Technology, Stockholm.

Perry, A.E., Henbest, S., Chong, M.S., 1986. A theoretical and experimental study of wall turbulence. J. Fluid Mech. 165, 163–199.

Robinson, S.K., 1991. The kinematics of turbulent boundary layer. NASA TM 103859.

Subramanian, C.S., Antonia, R.A., 1981. Effect of Reynolds number on a slightly heated turbulent boundary layer. Int. J. Heat Mass Transfer 24 (11), 1833–1846.

Satake, S., Kunugi, T., Takase, K., Ose, Y., Naito, N., 2003. Large scale structures of turbulent shear flow. In: Veidenbaum, A. et al. (Eds.), High Performance Computing. In: Lecture Notes in Computer Science, vol. 2858. Springer-Verlag, pp. 468–475.

Spalart, P.R., Moser, R.D., Rogers, M.M., 1991. Spectral methods for the Navier–Stokes equations with one infinite and two periodic directions. J. Comp. Phys. 96 (2), 297–324.

Tanahashi, M., Kang, S.-J., Miyamoto, S., Shiokawa, S., Miyauchi, T., 2003. Scaling of fine scale eddies in turbulent channel flows up to $Re_\tau = 800$. In: Proc. of the Third Symposium on Turbulent Shear Flow and Phenomana, Sendai, pp. 9–14.

Wei, T., Willmarth, W.W., 1989. Reynolds-number effects on the structures of a turbulent channel flow. J. Fluid Mech. 204, 57–95.

Wills, J.A.B., 1964. On convection velocities in turbulent shear flows. J. Fluid Mech. 20, 417–432.